

Leveraging graph neural networks and mobility data for COVID-19 forecasting

Fernando H. O. Duarte^a, Gladston J. P. Moreira^a, Eduardo J. S. Luz^a,
Leonardo B. L. Santos^b, Vander L. S. Freitas^{a,*}

^a*Department of Computing, Federal University of Ouro Preto, Morro do Cruzeiro, Ouro Preto, 35402-163, MG, Brazil*

^b*National Center for Monitoring and Early Warning of Natural Disasters, Estrada Dr. Altino Bondensan, 500, Sao Jose dos Campos, 12247-016, SP, Brazil*

Abstract

The COVID-19 pandemic has victimized over 7 million people to date, prompting diverse research efforts. Spatio-temporal models combining mobility data with machine learning have gained attention for disease forecasting. Here, we explore Graph Convolutional Recurrent Network (GCRN) and Graph Convolutional Long Short-Term Memory (GCLSTM), which combine the power of Graph Neural Networks (GNN) with traditional architectures that deal with sequential data. The aim is to forecast future values of COVID-19 cases in Brazil and China by leveraging human mobility networks, whose nodes represent geographical locations and links are flows of vehicles or people. We show that employing backbone extraction to filter out negligible connections in the mobility network enhances predictive stability. Comparing regression and classification tasks demonstrates that binary classification yields smoother, more interpretable results. Interestingly, we observe qualitatively equivalent results for both Brazil and China datasets by introducing sliding windows of variable size and prediction horizons. Compared to prior studies, introducing the sliding window and the network backbone extraction strategies yields improvements of about 80% in root means squared errors.

Keywords: Graph Neural Networks, Time series forecasting, Mobility networks, Backbone extraction, COVID-19

*Corresponding author

Email address: `vander.freitas@ufop.edu.br` (Vander L. S. Freitas)

1. Introduction

The COVID-19 pandemic, caused by SARS-CoV-2, was declared a pandemic by the World Health Organization (WHO) on March 11, 2020. On November 20, 2024, more than 776 million confirmed cases and approximately 7.1 million deaths were recorded globally. The first confirmed case in Brazil occurred on February 26, 2020, in São Paulo. Since then, the country has recorded more than 38 million confirmed cases and more than 700,000 deaths as of November 2024.

Droplets or aerosols transmit COVID-19, and those particles can remain suspended in the air, especially in closed and poorly ventilated environments. People’s mobility plays a crucial role in the spread of the virus. Public transport, for example, can become a favorable environment for contagion due to crowding and proximity between individuals. Understanding mobility patterns is essential to predict [1] and contain [2] the spread of the disease.

Spatio-temporal models that combine mobility data with machine learning (ML) have gained significant attention for COVID-19 forecasting. Recent work highlights the effectiveness of incorporating spatial and temporal dependencies through graph-based approaches. For example, [3] proposed an LSTM model enhanced by mobility data from Madrid’s bike-sharing system, achieving an 11.7% improvement in accuracy over baseline models without mobility features. Similarly, Witzke et al. [4] demonstrated that Graph Neural Networks (GNNs) using mobility data improved trend forecasting during Germany’s Omicron wave, particularly in identifying early change points where trends reversed direction.

Although the integration of mobility data improves accuracy, several limitations persist. Dense connectivity in mobility graphs often introduces noise, leading to less stable predictions, particularly in regression tasks. This issue is partially addressed in [5] through a spatio-temporal GNN incorporating both spatial and temporal edges. Still, the approach does not explore graph simplification techniques, such as backbone extraction, to filter out insignificant connections. Similarly, Sarkar et al. [6] focused on explainable GNN frameworks for identifying high-risk regions but relied primarily on static population features, neglecting dynamic relationships observed in mobility networks.

Li et al. [7] applied machine learning techniques, including GNN and XGBoost, to analyze the spread of COVID-19 in Southern California, integrating socioeconomic characteristics and regional mobility data. While

their approach demonstrated strong predictive performance, it relies on fixed temporal windows with weekly data, which limits adaptability to dynamic changes in disease transmission patterns. This rigid structure fails to capture the evolving nature of epidemic trends over time. In contrast, the use of sliding windows with variable lengths introduces overlapping temporal sequences, enhancing the robustness of predictions by capturing both short- and long-term dependencies. Furthermore, exploring variable window sizes and prediction horizons remains underexplored within the COVID-19 forecasting task.

Duarte *et al.* [8] leverage Graph Convolutional Network (GCN) models integrated with recurring neural networks (RNN) and long-short-term memory (LSTM) networks to analyze spatio-temporal data in a regression task, with the aim of improving temporal series prediction using complex networks. The predictions are performed at the node level, where each node represents a city. The GCN layer is interpreted as a graph comprising spatial information between cities and vehicle flows between them. Temporal series data of COVID-19 cases fed into RNNs or LSTMs with a fixed window size of 14 days to predict a number the next day. The specific models, GCRN (GCN+RNN) [9] and GCLSTM (GCN+LSTM) [10], encompass layers that use spatio-temporal data in complex neural networks.

Despite advances in ML-based forecasting, most studies formulate COVID-19 prediction as a regression task [8, 11, 12]. However, reframing the problem as a classification task [13] can provide significant benefits, such as simplified results, smoother predictions, and enhanced interpretability - particularly when categorizing outcomes into meaningful states, such as “stable” and “alert”. Furthermore, comparative analyses across multiple regional datasets remain limited despite their potential to uncover valuable insights into regional variations and shared patterns in disease dynamics. Moreover, the predominant focus on studies in a single region restricts the generalizability and broader applicability of the findings, highlighting the need for research in diverse geographic contexts [1, 6, 7, 8, 13, 12, 14, 15, 16, 17, 18].

From these identified gaps emerge several hypotheses. We posit that extracting the backbone [19, 20] of the mobility network can enhance accuracy by highlighting essential spatial relationships, that using sliding windows with overlapping sequences surpasses fixed-window approaches by capturing a richer temporal structure, that formulating the prediction task as binary classification (stable vs. alert states) produces more stable and interpretable results compared to regression; the consistent performance patterns across

prediction horizons and window sizes can be observed in datasets from both Brazil and China, demonstrating robustness to geographic variation; and that the GCRN and GCLSTM models perform comparably, validating the reliability of graph-based spatio-temporal forecasting methods in diverse contexts.

This work extends the study by Duarte *et al.* [8] by addressing these gaps and incorporating the above mentioned hypotheses into a comprehensive experimental framework. Our main contributions include (i) employing backbone extraction to filter out negligible connections and enhance predictive stability; (ii) introducing sliding windows of variable size and prediction horizons to capture temporal dependencies dynamically; (iii) comparing regression and classification tasks to demonstrate that binary classification yields smoother, more interpretable results; (iv) generalizing the approach to datasets of China and Brazil to evaluate the regional consistency; and (v) conduct a comparative analysis of their robustness and utility for the spatio-temporal prediction of COVID-19.

The remainder of this paper is organized as follows: Section 2 provides an overview of the materials and methods, including key definitions, datasets, and details of the employed methodology. Section 3 presents and discusses the results in the context of existing literature. Finally, Section 4 summarizes the findings and concludes the study.

2. Materials and methods

2.1. Mathematical preliminaries

A graph $G(V, E)$ has a set of vertices (nodes) $V = \{v_1, v_2, \dots, v_N\}$ and edges (links) E , totaling $N = |V|$ nodes and $L = |E|$ edges. Mathematically, the adjacency matrix $\mathbf{A} \in \mathbb{R}^{N \times N}$ provides the corresponding wiring diagram, with $\mathbf{A}_{ij} = 1$ when nodes i and j are connected, or zero otherwise, for unweighted graphs. When it comes to weighted graphs, which is our case with mobility networks, a_{ij} might have different values to describe connections. The $\mathbf{D}_{ii} = \sum_j \mathbf{A}_{ij}$ is the degree matrix, with zeros outside the main diagonal, and $\mathbf{X} \in \mathbb{R}^{N \times C}$ is the feature vector with C dimensions for each vertex, i.e., the input data for training the models.

2.2. Network Backbone extraction

A node might have connections that are not statistically relevant, which could deteriorate the results of regression and classification tasks. One pos-

sibility is to contrast such connections with the random expectation:

$$p_{ij} = \left(1 - \frac{\mathbf{A}_{ij}}{s_i}\right)^{k_i-1}, \quad (1)$$

in which k_i and s_i are the degree and strength of node i , respectively, and \mathbf{A}_{ij} is the weight of link ij [19]. The degree $k_i = \sum_{j=1}^N \theta(\mathbf{A}_{ij})$ denotes the number of connections node i has, with θ being the heaviside step function. Similarly, the node strength $s_i = \sum_{j=1}^N \mathbf{A}_{ij}$ is the weight accumulated by neighboring nodes.

The link is preserved if p_{ij} is below a desired significance level α . Otherwise, it is removed. Thus, the lower α , the sparser the network. In addition, one has to consider that each link has two ends, i and j , which requires choosing one via a criterion such as the largest or smallest. In this work, we pick the smallest, which leads to sparser networks.

2.3. Graph Convolutional Networks

In recent years, graph neural networks (GNNs) have emerged to handle graph-structured data in classification and regression problems at the node, edge, and graph levels [21]. GNNs are categorized into several types, such as recurrent (RecGNNs), convolutional (GCNs), autoencoders (GAEs), and spatio-temporal (STGNNs).

The GCNs are a specific type that adapts the convolution task, well-known in the Euclidean domain with images, to the non-Euclidean domain, where the notion of neighborhood occurs at the graph level [22]. Each node has a computational network, a subgraph that considers the aggregation operations with its neighborhood up to a chosen level of depth. As nodes with many neighbors propagate more quickly than more isolated nodes [23], one assigns greater weights to the features of nodes with fewer neighbors, thus balancing the influences.

Concerning node v , the first layer receives its features x_v , so the corresponding activation is $h_v^0 = x_v$. Then, for every consecutive layer, one combines data from its neighbors $N(v)$, sums it with its current activation, and does it recursively until reaching the final layer k , where the node em-

beddings $z^{(v)}$ can be retrieved:

$$\begin{cases} h_v^0 = x_v, \\ h_v^k = \sigma \left[W_k \sum_{u \in \mathcal{N}(v)} \left(\frac{h_u^{k-1}}{|\mathcal{N}(v)|} \right) + B_k h_v^{k-1} \right], \\ z^{(v)} = h_v^k, \end{cases} \quad (2)$$

so that B_k is the weight associated with the node itself, W_k is the weight matrix of the layer k , and σ is the activation function. For the matrix form of Eq. (2), let $\hat{A} = A + I_N$, A be the weighted adjacency matrix of the subgraph, I_N be the identity matrix of order N , and \hat{D} be the diagonal degree matrix of \hat{A} . The output of the convolution layer $k + 1$ is as follows:

$$H^{k+1} = \sigma(\hat{D}^{-1/2} \hat{A} \hat{D}^{-1/2} H^k W^{k+1}). \quad (3)$$

2.4. Time series prediction

To predict a future sequence of length F (prediction horizon), one feeds the model with a sequence of length l (window size) of observed data at previous timestamps:

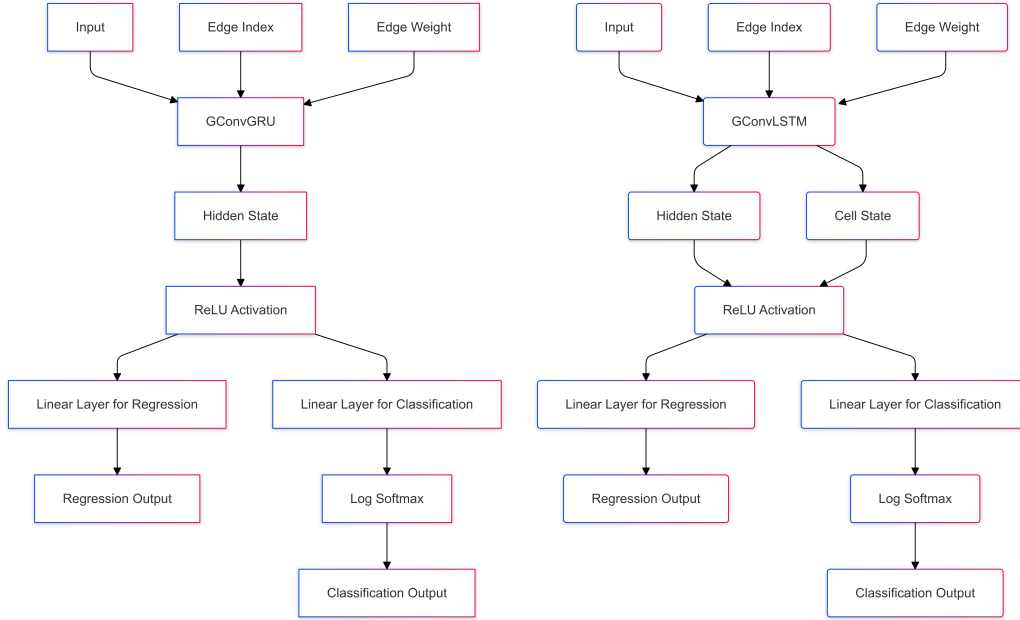
$$\hat{x}_{t+1}, \dots, \hat{x}_{t+F} = \max_{x_{t+1}, \dots, x_{t+F}} P(x_{t+1}, \dots, x_{t+F} | x_{t-l+1}, \dots, x_t), \quad (4)$$

where x_t is a snapshot at time t of the features and \hat{x}_t is the prediction.

In this setup, x_t represents the time series value in time t between all nodes within a static, directed, and weighted graph. In contrast, a snapshot X is a matrix $X \in \mathbb{R}^{N \times C}$, which captures data from time series at C time points.

2.5. GNNs for time series prediction

Graph Convolutional Recurrent Networks (GCRN) architectures [9] (Fig. 1a) and Graph Convolutional LSTM (GCLSTM) [10] (Fig. 1b) are Graph Neural Networks (GNNs) that deal with sequential data. The GCRN combines graph convolutions with temporal recurrence, while the GCLSTM employs LSTM units to model temporal dynamics on graphs. Each architecture is adapted to support regression and classification tasks, differing only in the output layer: *Linear* for regression and *Softmax* for classification.



(a) GCRN model architecture.

(b) GCLSTM model architecture.

Figure 1: Simplified representation of the GCRN and GCLSTM models.

The GConvLSTM (Graph Convolutional Long Short-Term Memory) and GConvGRU (Graph Convolutional Gated Recurrent Unit) layers are extensions of classical recurrent architectures (LSTM and GRU, respectively) for graph-structured data. Both combine the ability to model temporal sequences with the ability to capture spatial relationships.

The GConvLSTM layer uses graph convolutions to process sequences of data on graphs. Its main features include:

- **Input and output:** Receives node data, edge indices, and optionally edge weights. Produces hidden and cell states.
- **Graph Convolution:** Utilizes graph convolution to capture interactions between the graph’s nodes.
- **Laplacian Normalization:** Employs different normalization schemes to control information propagation.
- **Gate Computation:** Computes input, forget, cell, and output gates using graph convolutions and standard LSTM operations.

- State Updates: Updates hidden and cell states by integrating graph information.

The GConvGRU layer, in turn, is based on the GRU architecture, offering a simpler alternative to GConvLSTM. Its main features include:

- Structure: Similar to GConvLSTM, but with fewer parameters.
- Gates: Uses update and reset gates.
- Gate Computation: Employs graph convolutions to compute the gates.
- State Update: Updates the hidden state more directly.

2.6. Datasets

2.6.1. Brazilian mobility network

The Brazilian Institute of Geography and Statistics (IBGE) [24] provides essential data for this study, including mobility and population information. The mobility data, derived from IBGE’s survey of intercity connections, allows the construction of a mobility network representing flows between cities. This network is composed of $N = 5385$ vertices (cities) and $L = 65639$ edges (routes), where the weight of each edge corresponds to the frequency of vehicles outgoing between two cities in a typical week. These frequencies account for different modes of transportation, such as roads, waterways, and informal transport. Attributes such as travel time and cost were available, but were not incorporated into the analysis. In addition, population data from the 2022 Census, provided by IBGE, enhance the mobility network by facilitating the standardization of infection and mortality rates at the municipal level per 100,000 inhabitants.

2.6.2. Chinese mobility network

The Baidu Mobility Data [25] contains daily inflows and outflows of people between origins and destinations within 340 Chinese cities. The two adjacency matrices contain the rate of people who commute from i to j , having j as a reference (inflows), and the rate from j to i (outflows). In both cases, considering a reference city, its inflows or outflows sum up to one. In addition, each city has at most 100 neighbors. We aggregated the inflows from January to February 2020 and created a static mobility graph that reflects the average values during this period.

2.7. COVID-19 time series

For the Brazilian case, we used the publicly available COVID-19 temporal dataset provided by [26]. This dataset contains daily records of infections and deaths at Brazil’s municipal and state levels, with official information from the Ministry of Health. The data span from February 2020 to March 2023, covering a total of 1095 days. It includes geolocation information for cities, facilitating integration with the mobility network to better understand the dynamics of disease spread.

The Chinese time series covers a 694-day period from January 19, 2020, to December 12, 2022. The COVID-19 time series contains cases for only 205 of the 340 cities of the mobility data discussed in Section 2.6.2. We then only used those 205 nodes.

2.8. Experimental setup

2.8.1. Data organization and standardization

The temporal data were standardized using the *z-score*, a method that transforms the values of a variable to a scale with a mean of zero and a standard deviation of one:

$$z = \frac{x - \mu}{\sigma} \quad (5)$$

where x is the input value, μ is the mean, and σ is the standard deviation. This standardization ensures that the data are on the same scale, which benefits the models’ training.

The graph was backbone extracted for Brazil, reducing the initial number of edges above 65,000 to just above 20,000. For this, we use $\alpha = 0.01$ and ensure that at least the 5 most weighted connections of each node are retained to ensure that no city was excluded from the analysis. In the end, we have snapshots of the data, where each city (there are 5,385 in total) is represented by a time series spanning 1,095 days with information on reported COVID-19 cases.

In the case of China, the backbone extraction of our graph initially comprised 205 nodes and 19,046 edges. Using the same method with identical settings, we achieved a substantial decrease in the number of edges, culminating in slightly more than 980 connections between all 205 vertices.

2.8.2. Train and test data split

Figure 2 shows the data preprocessing pipeline, which transforms data into snapshots that serve as input to neural network models. Of these snapshots, 80% are allocated for training and the remaining 20% for testing.

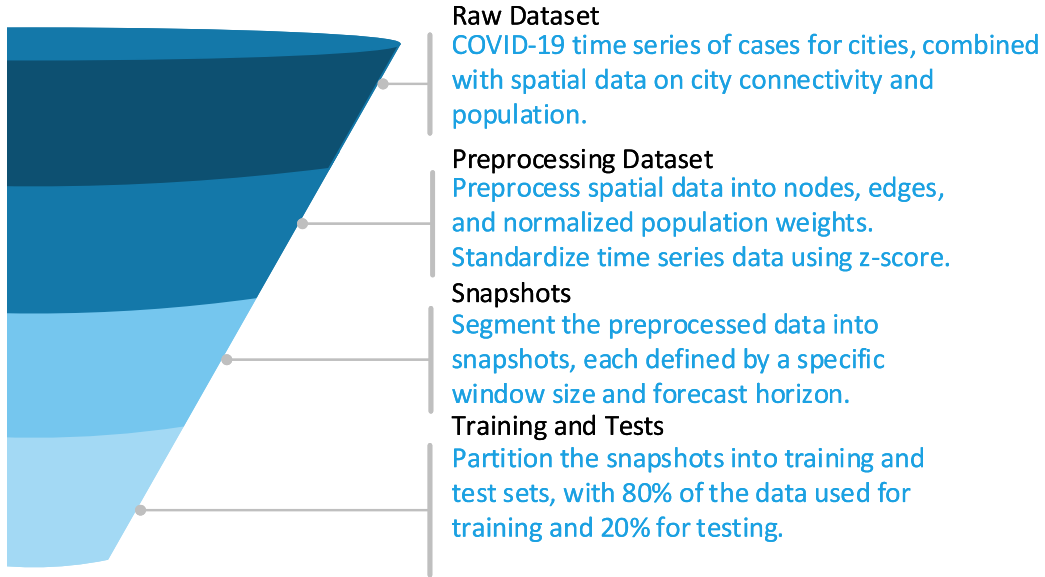


Figure 2: Data Preprocessing Workflow.

Taking into account a temporal dataset that covers 1,095 days, the division for Brazil results in 876 days allocated for training and 219 days for testing. For China, out of a total of 694 days, 555 are for training and 139 for testing. The application of sliding windows offers flexibility in the number of snapshots generated, which is which is adaptable to various experimental setups.

2.8.3. Evaluation metrics

For regression, we use the Root Mean Squared Error (RMSE):

$$RMSE = \sqrt{\frac{1}{n} \sum_{i=1}^n (y_i - \hat{y}_i)^2} \quad (6)$$

where y_i is the real value, \hat{y}_i is the prediction, and n is the number of samples.

Concerning classification, we use the following.

- F1-Score: Harmonic combination of precision and recall, as follows:

$$F1 = 2 \cdot \frac{\text{Precision} \cdot \text{Recall}}{\text{Precision} + \text{Recall}} \quad (7)$$

- Precision: proportion of true positives among the predicted positives:

$$\text{Precision} = \frac{TP}{TP + FP} \quad (8)$$

where TP is the number of true positives, and FP represents false negatives.

- Recall: Proportion of true positives among the actual positive cases:

$$\text{Recall} = \frac{TP}{TP + FN} \quad (9)$$

where FN is the number of false negatives.

2.8.4. Experiments

We build on the results of Duarte *et al.* [8] by using the Brazilian mobility network and COVID-19 time series of cases and the neural architectures GCLSTM and GCRN. The parameters are the same, with a window size of 14 days and a prediction horizon of 1 day, and without employing the sliding window strategy, we end up with a sequence of non-overlapping time series segments of size 15. The following experiments pile up different strategies to improve the results:

- We first reproduce the results of Duarte *et al.* [8];
- Experiment 1: Next, we include 4 additional months of data (December 2022 to March 2023);
- Experiment 2: Then, we add the sliding window strategy, so the number of samples increases for training and testing;
- Experiment 3: Finally, we extract the backbone from the mobility network to consider only the most significant neighbors of each node, as described in Section 2.2.

The following experiments are carried out on the Brazilian and Chinese datasets. Using the last strategy, which consists of employing a sliding window and extraction of the network backbone, we now vary both the window size and the prediction horizon from 1 to 14 days so we can capture their dependency. Each snapshot combines temporal and spatial (graph) data for a specific interval. Considering all possible combinations of windows and horizons, we end up with 196 different cases (14×14):

- Experiment 4: Regression for Brazil;
- Experiment 5: Regression for China;

In addition to the regression task of predicting future time series values, we also forecast its tendency via a classification task. This approach is motivated by the work of The Harvard Global Health Institute and Harvard’s Edmond J. Safra Center for Ethics [27], which has participated in a collaborative effort with a network of research and policy organizations to achieve consensus on key metrics to evaluate the status of response to the pandemic and key performance indicators to assess the effectiveness of response tools deployed. They define risk levels based on new daily cases per 100k population, using a seven-day rolling average and a trend direction and rate. After that, they represent the following four risk levels:

- Red: More than 25 daily new cases per 100k people;
- Orange: Between 10 and 25 daily new cases per 100k people;
- Yellow: Between 1 and 10 daily new cases per 100k people;
- Green: Less than 1 daily new case per 100k people.

We initially attempted to apply the same method with four classes for each time series of Brazil and China at the city level. However, this resulted in an imbalance between the classes, prompting us to modify the approach to encompass just two classes, which we called *Stable* and *Alert*, by employing an adaptation of the work of [27].

For each time series, we calculated the classification targets using a custom function based on the previous seven days of data. The key steps in the target computation are as follows:

- Sliding window for moving average: We computed a 7-day moving average for all cities for each day in the dataset. This moving average captures the smoothed trend in the data over the past week and helps to reduce noise in the daily variations.
- Normalization per 100k Inhabitants: To make the values comparable across cities with different population sizes, the moving average was normalized to the population size of 100,000 inhabitants. This was achieved by dividing the moving average by the normalized population, which is pre-computed for each city.
- Trend calculation using Linear Regression: To incorporate the recent trend in the data, we performed a linear regression over the past 7 days for each city. The regression estimated the trend rate as the slope of the best-fit line, representing the rate of change in cases over the window.
- Combining metrics: The normalized moving average was then multiplied by the computed trend rate to produce a combined metric for each city. This metric captures both the current level of cases and their recent growth rate.
- Binary labeling based on threshold: The combined metric was compared against a predefined threshold of 10. If the metric exceeded the threshold, the city was classified as *Alert* (class 1). Otherwise, it was classified as *Stable* (class 0). This binary classification approach simplifies interpretation and focuses on distinguishing stable situations from alert-worthy ones.

By applying this methodology across all cities in the dataset, we produced a consistent and interpretable set of binary classification targets for each day in the time series. This approach effectively captures both the absolute number of cases (normalized for the population) and the recent dynamics of case trends, ensuring that the classification is in line with public health priorities.

The number of samples per class is relatively balanced between *Stable* and *Alert*, with about 47% of samples with the *Alert* label and 53% *Stable* for Brazil, while China has 45% of *Alert* and 55% for *Stable*. The last two experiments are the following:

- Experiment 6: Classification for Brazil;

- Experiment 7: Classification for China.

In this final stage of the study, the same model that was previously used for regression is now used for a classification test. The model has been adapted to predict the two classes (stable and alert) over time series. The output of the classification model is the probability of each class, which is calculated using the logarithm of the softmax function (LogSoftmax).

3. Results

3.1. Building on previous results

Table 1 presents the results for the first three experiments, based on Duarte et al. [8]. The RMSE is computed for each time stamp in the test set, where each time stamp corresponds to predictions for a set of many cities. This strategy allows us to evaluate the model’s error across all cities at each time stamp, capturing its behavior over time. From the resulting RMSE values, we compute the mean, standard deviation, minimum, and maximum RMSE to summarize the performance of the model over the entire test period. First, one starts without the sliding window technique to have a setup comparable to their work but with more 4 months of data. The results demonstrate a significant reduction in RMSE, with GCLSTM errors dropping from 3535.38 to 2268.27. Concerning GCRN, errors dropped from 2990.40 to 2102.27. When we add the sliding window strategy, the amount of data increases, and errors decrease even more, reaching 1150.35 for GCLSTM and 1315.47 for GCRN. When excluding the extraction of the network backbone, the GCLSTM model reaches an RMSE of 682.14 (80.7% reduction), and GCRN achieves 560.92 (a decrease of 81.2%).

There is a progressive improvement in results as new techniques are applied, highlighting the effectiveness of sliding window and backbone extraction strategies.

3.2. Regression performance

Figure 3 presents the comparative results of Experiment 4 between the GCRN and GCLSTM models in regression tasks, considering different window sizes (1 – 14) and prediction horizons (1 – 14) for Brazil.

Regarding overall performance, the models showed remarkably similar results regarding the Root Mean Square Error (RMSE). This is evidenced in

Table 1: Results for GCLSTM and GCRN models with different configurations, using a window size of 14 and prediction horizon of 1.

Model	Scenario	Mean RMSE	Std	Min	Max
GCLSTM	Duarte <i>et al.</i> [8]	3535.38	1179.61	1337.55	5327.53
	Exp. 1: more data	2268.27	1189.09	1050.93	4564.23
	Exp. 2: sliding window	1150.35	924.28	443.17	4549.68
	Exp. 3: sliding window; backbone	682.14	950.88	249.75	4059.08
GCRN	Duarte <i>et al.</i> [8]	2990.40	1000.01	1178.76	4598.27
	Exp. 1: more data	2102.27	1336.78	804.79	4743.18
	Exp. 2: sliding window	1315.47	852.58	709.11	4560.40
	Exp. 3: sliding window; backbone	560.92	875.39	150.23	4173.21

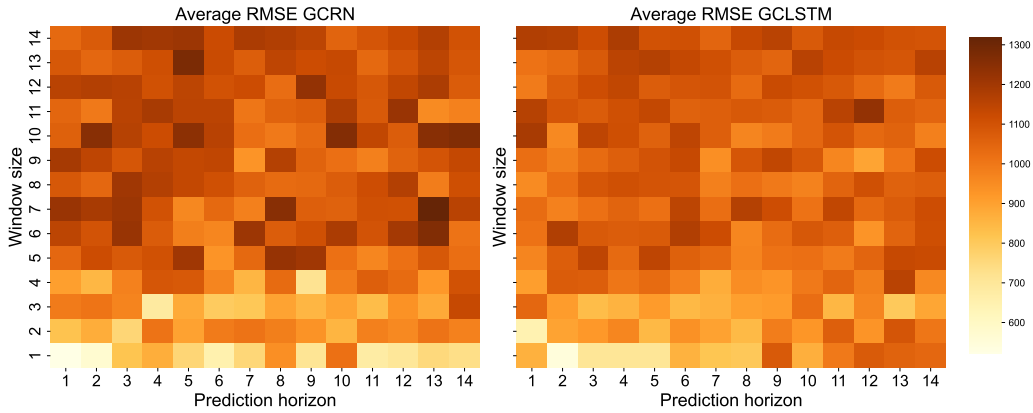


Figure 3: Experiment 4: Average RMSE Heatmaps for Regression Task, Brazil.

Table 2: Experiment 4: Performance Comparison between Models

Statistic	GCRN	GCLSTM
Maximum RMSE	1319.05	1228.81
Minimum RMSE	520.92	548.02
Mean RMSE	1048.06	1030.66
Standard Deviation RMSE	140.95	106.02
1st Quartile RMSE	984.12	979.20
Median RMSE	1072.72	1053.12
3rd Quartile RMSE	1147.40	1101.07

Table 2, where the slight difference in means ($\Delta = 17.40$) and standard deviations ($\Delta = 34.93$) indicates that both models have comparable predictive

capabilities.

The quartile analysis reveals a very similar error distribution between the GCRN and GCLSTM models, with the first quartile, median, and third quartile having close values, suggesting consistent performance across various forecasting conditions. When examining the range of errors, some interesting characteristics emerge: the GCRN shows more significant variability in its results, with a range of 798.13 (spanning from 520.92 to 1319.05). At the same time, the GCLSTM demonstrates a slightly more constrained error range of 680.79 (from 548.02 to 1228.81).

The standard deviation provides additional information about the model error distributions. The GCRN exhibits a standard deviation of 140.95, indicating more spread in the error values, while the GCLSTM shows a standard deviation of 106.02, suggesting more concentrated error distributions. The mean RMSE values are particularly close, with the GCRN at 1048.06 and the GCLSTM at 1030.66, further highlighting the models' comparable performance.

This analysis suggests that while the GCLSTM model shows slightly more consistent performance with a lower standard deviation, both models perform comparably in predicting the time series data, with only marginal differences in their predictive capabilities.

Both models exhibit a common trend of performance degradation as the prediction horizon increases, indicating that forecasting further into the future is a more challenging task. When comparing the variability of the predictions, the GCRN showed greater instability, particularly in long-term horizons, whereas the GCLSTM showed greater consistency. This difference suggests that the GCLSTM may be more robust and better able to generalize to unseen data.

Figure 4 shows the results for China, which, unlike the observed for Brazil, did not show a defined pattern, and there are some outliers, such as for GCLSTM with both window size and prediction horizon of 5.

In the China results Table 3, the GCRN and GCLSTM models displayed similar statistical characteristics. The most noticeable difference lies in the maximum RMSE values, where the GCLSTM model shows a significantly higher maximum error (762.37) than the GCRN model (401.35). This suggests that while both models perform similarly under most conditions, the GCLSTM has occasional predictions with substantially higher errors.

The standard deviation further highlights the models' different error distributions. The GCRN's lower standard deviation of 73.81 indicates more

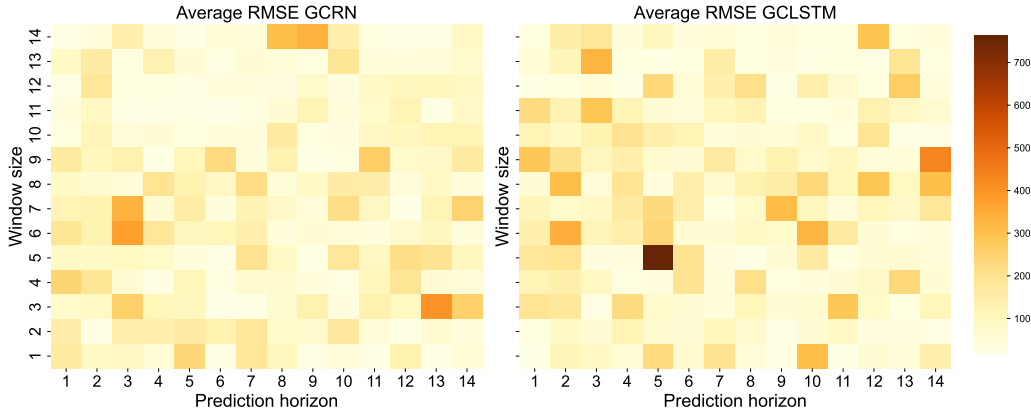


Figure 4: Experiment 5: Average RMSE Heatmaps for Regression Task, China.

Table 3: Performance Comparison between Models in China

Statistic	GCRN	GCLSTM
Maximum RMSE	401.35	762.37
Minimum RMSE	16.22	16.41
Mean RMSE	96.65	109.09
Standard Deviation RMSE	73.81	95.55
1st Quartile RMSE	40.02	38.65
Median RMSE	80.52	77.65
3rd Quartile RMSE	133.75	148.93

consistent predictions, while the GCLSTM’s higher standard deviation of 95.55 suggests more variable performance. The GCRN model showed a more constrained range of RMSE values, spanning from 16.22 to 401.35, with a mean of 96.65 and a standard deviation of 73.81. In contrast, the GCLSTM model exhibited more significant variability, with RMSE values ranging from 16.41 to 762.37, a mean of 109.09, and a standard deviation of 95.55.

3.3. Classification performance

Concerning Experiment 6 - classification with the Brazilian dataset -, both models perform better for shorter prediction horizons with larger window sizes. Observing the heatmaps for the F1-Score, Precision, and Recall metrics (Figures 5, 6, and 7), this outcome was expected. The GCRN model achieves maximum scores of 86% for F1-Score, Precision, and Recall (window

size 8, prediction horizon 1), while the GCLSTM reaches 83% (window size 3, prediction horizon 1). From a window size of 5 onward, an improvement in all metrics is observed, with the GCRN consistently peaking at a window size of 8 with a prediction horizon of 1. Some key observations are:

- GCRN demonstrates more stable performance across different configurations.
- GCLSTM exhibits slightly greater volatility in performance.
- Both models show a degradation in performance as the prediction horizon increases.
- Smaller window sizes (1-4) produce poorer results for both models.
- The worst results are close to 50%.
- Window sizes between 6-10 yield the best results for both models.

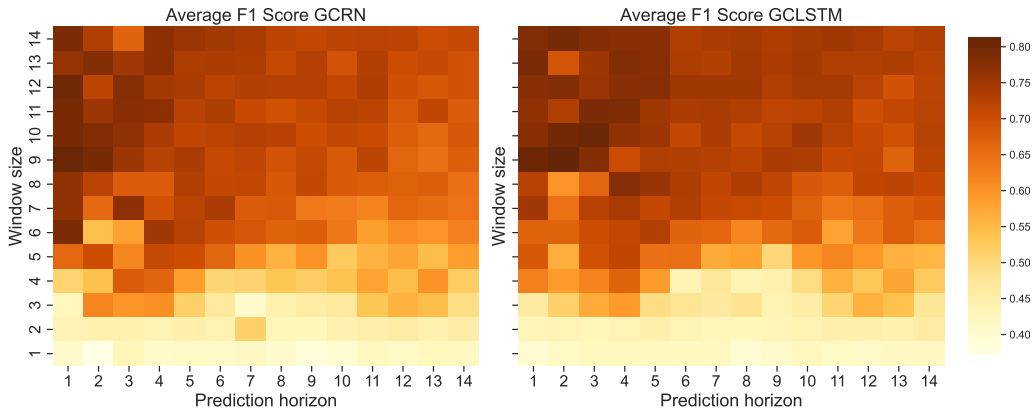


Figure 5: Experiment 6: Average F1-Score Heatmaps for Classification Task, Brazil.

Table 4 presents a general comparison of classification performance metrics for the GCRN and GCLSTM models, highlighting the best values among the models.

Starting with the F1-Score, the GCRN model achieves a maximum value (0.86) compared to the GCLSTM (0.83). This pattern is consistent when analyzing Precision and Recall. The same holds true for the minimum values, means, and standard deviations in the three metrics, indicating a balance of

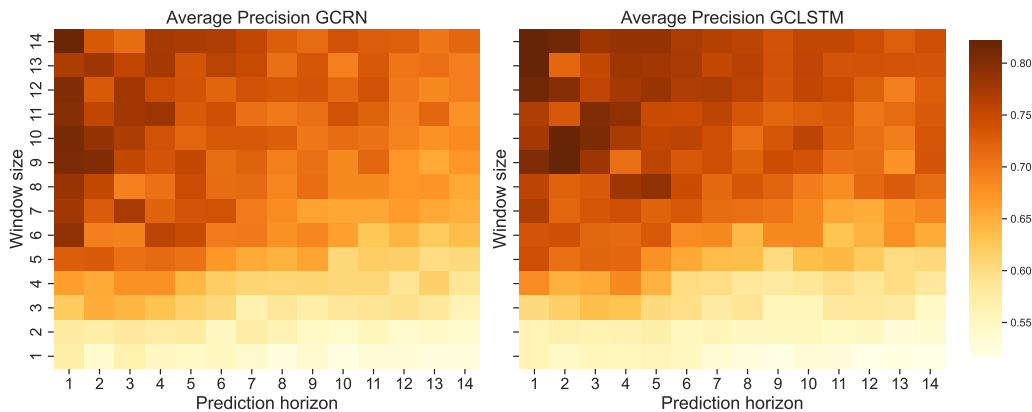


Figure 6: Experiment 6: Average Precision Heatmaps for Classification Task, Brazil.

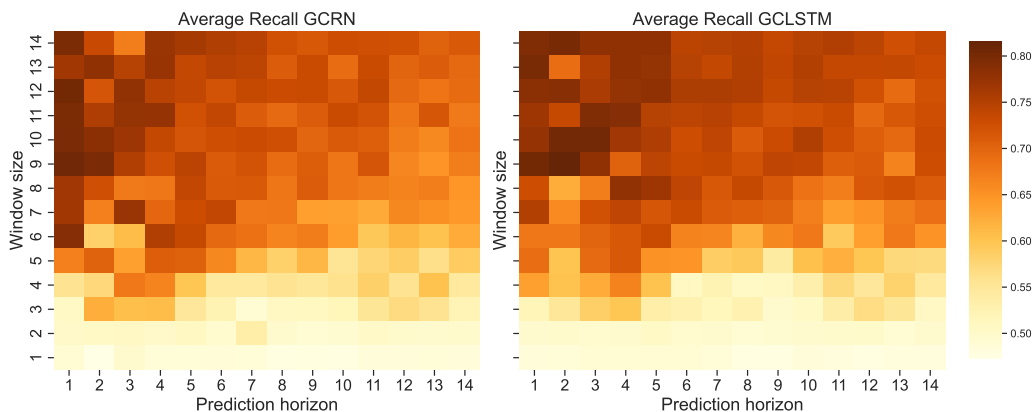


Figure 7: Experiment 6: Average Recall Heatmaps for Classification Task, Brazil.

performance between the models. Quartile statistics reveal a very similar distribution between the two models, with a median of 0.68 for GCRN and 0.69 for GCLSTM.

The GCRN and GCLSTM models showed very similar performance in all metrics analyzed. However, GCLSTM demonstrates slightly better average performance (mean and median) in precision and recall. However, the GCRN exhibits greater performance stability, with a lower standard deviation across all metrics.

Concerning Experiment 7, the performance analysis of the GCRN and GCLSTM models for the China dataset reveals in the heatmaps for F1-score (Figure 8), precision (Figure 9), and recall (Figure 10) performance values

Table 4: Experiment 6: Classification Metrics, Brazil.

Metric	F1-Score		Precision		Recall	
Statistic	GCRN	GCLSTM	GCRN	GCLSTM	GCRN	GCLSTM
Maximum	0.86	0.83	0.86	0.84	0.86	0.83
Minimum	0.35	0.35	0.48	0.47	0.46	0.45
Mean	0.64	0.64	0.68	0.69	0.65	0.66
Std. Dev.	0.12	0.13	0.08	0.09	0.10	0.11
1st Quartile	0.55	0.53	0.61	0.61	0.57	0.56
Median	0.68	0.69	0.69	0.71	0.68	0.69
3rd Quartile	0.73	0.74	0.74	0.76	0.73	0.75

ranging between 0.94 and 0.98 for both models.

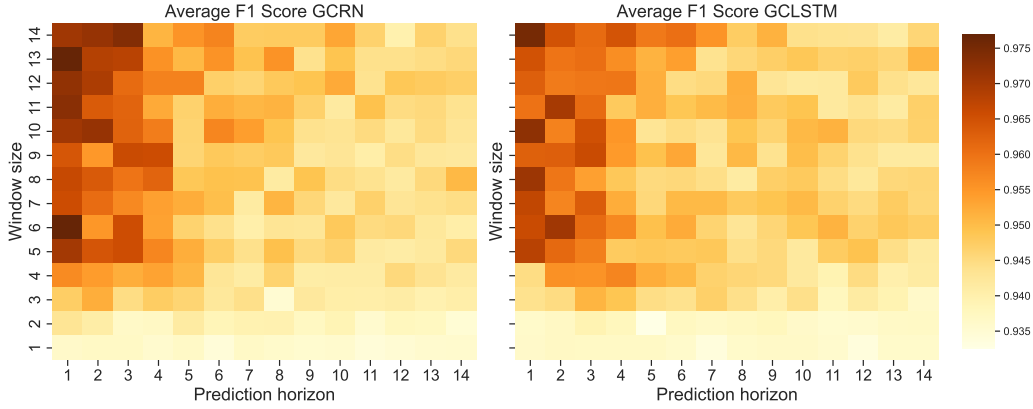


Figure 8: Average F1-Score Heatmaps for Classification Task, China.

The average F1-score of the GCLSTM remains consistently at 0.96, with a standard deviation of only 0.01, while the GCRN shows a variation of 0.02. In precision metrics, a gradual reduction of approximately 3% is observed in longer prediction horizons, with the GCLSTM decreasing from 0.97 to 0.94 and the GCRN from 0.96 to 0.92. This decline is particularly pronounced after the tenth prediction horizon, highlighting the increasing challenges in long-term forecasting.

The comparative analysis of the two models suggests that both are effective for the classification task in the China dataset. The GCLSTM stands out for its more uniform performance, with a coefficient of variation 33% lower

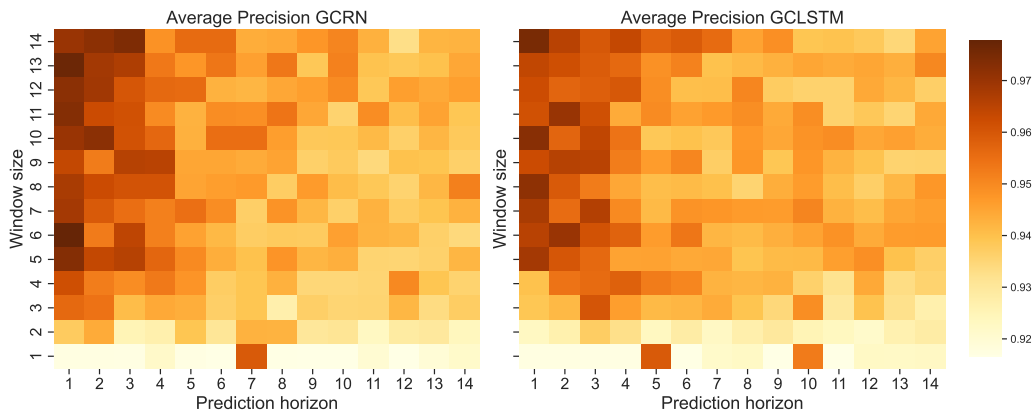


Figure 9: Average Precision Heatmaps for Classification Task, China.

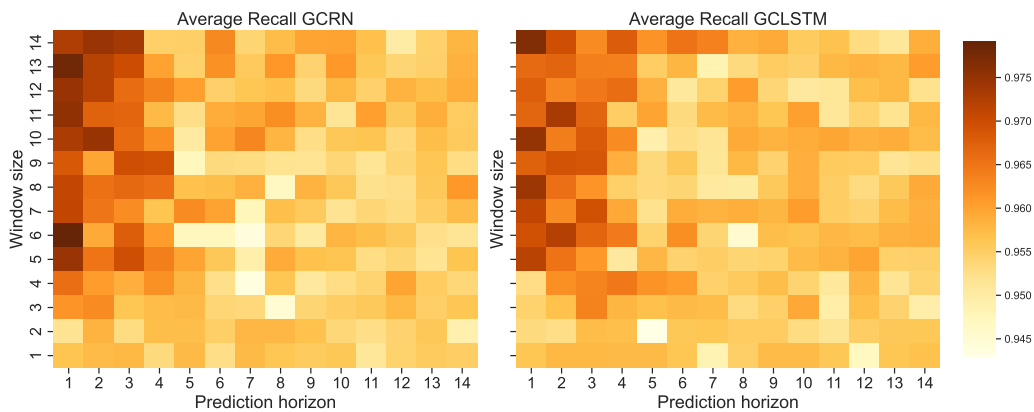


Figure 10: Average Recall Heatmaps for Classification Task, China.

than that of the GCRN. The results demonstrate statistical robustness, with 92% of predictions remaining above 0.94, indicating significant adaptability to the specific context of classification for Chinese data.

4. Conclusions

We investigate the interplay of window size and prediction horizons when forecasting time series of COVID-19 cases at the node level of mobility networks, exploring regression and classification of trends. As case studies, we used data from Brazil and China during the COVID-19 pandemic. Regarding Brazil, the mobility data consist of cities connected by their flow of

Table 5: Experiment 7: Classification Metrics, China

Metric	F1-Score		Precision		Recall	
Statistic	GCRN	GCLSTM	GCRN	GCLSTM	GCRN	GCLSTM
Maximum	0.98	0.98	0.98	0.97	0.98	0.98
Minimum	0.93	0.93	0.92	0.92	0.94	0.94
Mean	0.95	0.95	0.94	0.94	0.96	0.96
Std. Dev.	0.01	0.01	0.01	0.01	0.01	0.01
1st Quartile	0.94	0.94	0.94	0.94	0.95	0.95
Median	0.95	0.95	0.94	0.94	0.96	0.96
3rd Quartile	0.95	0.95	0.95	0.95	0.96	0.96

vehicles during a regular week. For China, the links represent the rates of people moving from one city to another. Concerning neural architectures, we use GCRN [9] and GCLSTM [10], combinations of Graph Convolutional Networks (GCNs) and Recurrent Neural Networks (RNNs) and Long Short-Term Memory (LSTM) to predict time series at the node level. Both architectures are trained to perform regression and classification tasks. In the former, they predict the exact number of future cases per municipality. At the same time, in the latter, they determine whether a municipality is in an alert or stable state, considering a normalization per 100,000 inhabitants for a fairer comparison.

Unlike previous literature [8], a significant improvement is observed when we extract the backbone of the mobility network, which keeps only the most significant connections between municipalities. We also adopt a sliding window approach to train the models, which, combined with the network backbone, reduces the mean RMSE by approximately 80%.

As part of the experiments, we vary the input window size and the prediction horizons to investigate their interplay, showing that smaller horizons and larger windows produce better results for classification, with an F1-score consistently above 0.5 for Brazil and 0.9 for China. The pattern is qualitatively the same for both countries, showing the validity of the methodology employed in different contexts and data complexity since the Chinese network used has 205 nodes and the Brazilian network has 5385. However, trends are not evident in regression, probably due to the complex coupling between neighboring nodes.

For future work, it would be valuable to explore alternative backbone

extraction techniques [20] to determine whether different neighborhoods exhibit distinct behaviors. This could be combined with alternative neural network architectures for time series forecasting [28]. Additionally, investigating graph-based model explainability could help identify the most critical subgraphs for each node, as well as the features (input points) that best explain the results. Such analyses could also be conducted separately for each transport mode, including terrestrial, aerial, and fluvial systems.

Acknowledgments

This work was supported by the Conselho Nacional de Desenvolvimento Científico e Tecnológico (CNPq, grants 307151/2022-0, 308400/2022-4, 441016/2020-0), Fundação de Amparo à Pesquisa do Estado de Minas Gerais (FAPEMIG, grants APQ-01518-21, APQ-01647-22), and Coordenação de Aperfeiçoamento de Pessoal de Nível Superior – Brasil (CAPES) - Finance Code 001. We also extend our thanks to the Universidade Federal de Ouro Preto (UFOP) for their invaluable support.

Author contributions: CRediT

Fernando H. O. Duarte: Investigation, Methodology, Software, Validation, Visualization, Writing – original draft; **Gladston J. P. Moreira:** Resources, Supervision, Methodology, Funding acquisition, Validation, Writing – review & editing; **Eduardo J. S. Luz:** Investigation, Methodology, Resources, Validation, Writing – review & editing; **Leonardo B. L. Santos:** Writing – review & editing; **Vander L. S. Freitas:** Conceptualization, Investigation, Methodology, Project administration, Supervision, Software, Validation, Writing – review & editing.

Declaration of generative AI and AI-assisted technologies in the writing process

Statement: During the preparation of this work the author(s) used ChatGPT in order to translate some sentences from PT-BR to American EN. After using this tool/service, the author(s) reviewed and edited the content as needed and take(s) full responsibility for the content of the published article.

Data availability:

The datasets used and analyzed during the current study are publicly available and have been described in detail within the manuscript. The source code is available at: https://github.com/hodfernando/2024_ASOC_GNN_COVID19_Forecast.

References

- [1] V. L. S. Freitas, T. C. R. O. Konstantyner, J. F. Mendes, C. S. N. Sepetauskas, L. B. L. Santos, The correspondence between the structure of the terrestrial mobility network and the spreading of covid-19 in brazil, *Cadernos de Saúde Pública* 36 (2020) e00184820.
- [2] V. L. Freitas, G. J. Moreira, L. B. Santos, Robustness analysis in an inter-cities mobility network: modeling municipal, state and federal initiatives as failures and attacks toward sars-cov-2 containment, *PeerJ* 8 (2020) e10287.
- [3] M. Muñoz-Organero, P. Callejo, M. Á. Hombrados-Herrera, A new rnn based machine learning model to forecast covid-19 incidence, enhanced by the use of mobility data from the bike-sharing service in madrid, *Heliyon* 9 (6) (2023).
- [4] S. Witzke, N. Danz, K. Baum, B. Y. Renard, Mobility data improve forecasting of covid-19 incidence trends using graph neural networks, in: *epiDAMIK 6.0: The 6th International workshop on Epidemiology meets Data Mining and Knowledge Discovery at KDD 2023*, 2023.
- [5] A. Kapoor, X. Ben, L. Liu, B. Perozzi, M. Barnes, M. Blais, S. O'Banion, Examining covid-19 forecasting using spatio-temporal graph neural networks, *arXiv preprint arXiv:2007.03113* (2020).
- [6] S. Sarkar, A. Alhamadani, C.-T. Lu, Explainable prediction of the severity of covid-19 outbreak for us counties, in: *2022 IEEE International Conference on Big Data (Big Data)*, IEEE, 2022, pp. 5338–5345.
- [7] H. Li, R. Wei, W. Wang, N. Yu, Predicting covid-19 transmission in southern california with machine learning methods, in: *2024 9th International Conference on Big Data Analytics (ICBDA)*, IEEE, 2024, pp. 1–10.

- [8] F. H. O. Duarte, G. J. P. Moreira, E. J. S. Luz, L. B. L. Santos, V. L. S. Freitas, Time series forecasting of covid-19 cases in brazil with gnn and mobility networks, in: M. C. Naldi, R. A. C. Bianchi (Eds.), *Intelligent Systems*, Springer Nature Switzerland, Cham, 2023, pp. 361–375.
- [9] Y. Seo, M. Defferrard, P. Vandergheynst, X. Bresson, Structured sequence modeling with graph convolutional recurrent networks, in: *Neural Information Processing*, 2018, pp. 362–373.
- [10] J. Chen, X. Wang, X. Xu, Gc-lstm: graph convolution embedded lstm for dynamic network link prediction, *Applied Intelligence* 52 (7) (2022) 7513–7528.
- [11] C. Comito, C. Pizzuti, Artificial intelligence for forecasting and diagnosing covid-19 pandemic: A focused review, *Artificial Intelligence in Medicine* 128 (2022) 102286. doi:<https://doi.org/10.1016/j.artmed.2022.102286>.
URL <https://www.sciencedirect.com/science/article/pii/S0933365722000513>
- [12] R. P. Joshi, V. Pejaver, N. E. Hammarlund, H. Sung, S. K. Lee, A. Furmanchuk, H.-Y. Lee, G. Scott, S. Gombar, N. Shah, S. Shen, A. Nassiri, D. Schneider, F. S. Ahmad, D. Liebovitz, A. Kho, S. Mooney, B. A. Pinsky, N. Banaei, A predictive tool for identification of sars-cov-2 pcr-negative emergency department patients using routine test results, *Journal of Clinical Virology* 129 (2020) 104502. doi:<https://doi.org/10.1016/j.jcv.2020.104502>.
URL <https://www.sciencedirect.com/science/article/pii/S1386653220302444>
- [13] B. Pirouz, S. Shaffiee Haghshenas, S. Shaffiee Haghshenas, P. Piro, Investigating a serious challenge in the sustainable development process: Analysis of confirmed cases of covid-19 (new type of coronavirus) through a binary classification using artificial intelligence and regression analysis, *Sustainability* 12 (6) (2020). doi:[10.3390/su12062427](https://doi.org/10.3390/su12062427).
URL <https://www.mdpi.com/2071-1050/12/6/2427>
- [14] F. H. O. Duarte, G. J. Moreira, E. J. Luz, L. B. Santos, V. L. Freitas, Correlations between epidemiological time series forecasting and influence regions of brazilian cities, 2023, p. 363 – 368, cited by: 0.

URL <https://www.scopus.com/inward/record.uri?eid=2-s2.0-85181098306&partnerID=40&md5=f60d73eeee623d21c9b7119bbc4407319>

- [15] M. R. Davahli, K. Fiok, W. Karwowski, A. M. Aljuaid, R. Taiar, Predicting the dynamics of the covid-19 pandemic in the united states using graph theory-based neural networks, *International journal of environmental research and public health* 18 (7) (2021) 3834.
- [16] H. Xie, D. Li, Y. Wang, Y. Kawai, Visualization method for the spreading curve of covid-19 in universities using gnn, in: *2022 IEEE International Conference on Big Data and Smart Computing (BigComp)*, IEEE, 2022, pp. 121–128.
- [17] D. Fanelli, F. Piazza, Analysis and forecast of covid-19 spreading in china, italy and france, *Chaos, Solitons & Fractals* 134 (2020) 109761.
- [18] C.-P. Kuo, J. S. Fu, Evaluating the impact of mobility on covid-19 pandemic with machine learning hybrid predictions, *Science of The Total Environment* 758 (2021) 144151. doi:<https://doi.org/10.1016/j.scitotenv.2020.144151>. URL <https://www.sciencedirect.com/science/article/pii/S0048969720376828>
- [19] F. Menczer, S. Fortunato, C. A. Davis, *A First Course in Network Science*, Cambridge University Press, 2020. doi:[10.1017/9781108653947](https://doi.org/10.1017/9781108653947).
- [20] C. H. Gomes Ferreira, F. Murai, A. P. C. Silva, M. Trevisan, L. Vassio, I. Drago, M. Mellia, J. M. Almeida, On network backbone extraction for modeling online collective behavior, *PLOS ONE* 17 (9) (2022) 1–36. doi:[10.1371/journal.pone.0274218](https://doi.org/10.1371/journal.pone.0274218). URL <https://doi.org/10.1371/journal.pone.0274218>
- [21] Z. Wu, S. Pan, F. Chen, G. Long, C. Zhang, P. S. Yu, A comprehensive survey on graph neural networks, *IEEE Transactions on Neural Networks and Learning Systems* 32 (2021) 4–24. doi:[10.1109/TNNLS.2020.2978386](https://doi.org/10.1109/TNNLS.2020.2978386).
- [22] M. Niepert, M. Ahmed, K. Kutzkov, Learning convolutional neural networks for graphs, in: *International conference on machine learning*, PMLR, 2016, pp. 2014–2023.

- [23] T. N. Kipf, M. Welling, Semi-supervised classification with graph convolutional networks, arXiv preprint arXiv:1609.02907 (2016).
- [24] IBGE, Ligações rodoviárias e hidroviárias: 2016, IBGE, Coordenação de Geografia Rio de Janeiro, Brazil, 2017.
- [25] China Data Lab, Baidu Mobility Data (2020). doi:10.7910/DVN/FAEZIO.
URL <https://doi.org/10.7910/DVN/FAEZIO>
- [26] W. Cota, Monitoring the number of covid-19 cases and deaths in brazil at municipal and federative units level, SciELO Preprints (2020).
- [27] Harvard Global Health Institute and Harvard’s Edmond J. Safra Center for Ethics, Key metrics for covid suppression a framework for policy makers and the public (2020).
- [28] M. Jin, H. Y. Koh, Q. Wen, D. Zambon, C. Alippi, G. I. Webb, I. King, S. Pan, A survey on graph neural networks for time series: Forecasting, classification, imputation, and anomaly detection, IEEE Transactions on Pattern Analysis and Machine Intelligence 46 (12) (2024) 10466–10485. doi:10.1109/TPAMI.2024.3443141.